Identification of Scattering Objects in Microcell Urban Mobile Propagation Channel

Mir Ghoraishi, *Member, IEEE*, Junichi Takada, *Member, IEEE*, and Tetsuro Imai, *Member, IEEE*

***Abstract*—A series of measurements in two streets in a dense urban area were accomplished. The measurement scenario was small microcell line-of-sight (LoS) with low antenna height at both link ends where dipole sleeve transmitter (Tx) antenna, directive receiver (Rx) antenna, wideband pseudo-noise (PN) signal and correlator were employed. We analyze the data obtained from the measurements by careful investigation of the single-bounce scattering power distribution conforming to precise maps of the environments including all present objects. We try to identify the single-bounce scatterers for the cluster received waves appearing in the single-bounce scattering power distribution. A number of objects were identified by this method as single-bounce scatterers within the spatial resolution bins. The identified objects are signboards, traffic signs, etc. and we conclude that any metallic object visible to both Tx and Rx with dimensions in orders of tens of wavelengths can be a significant source of scattering in small cell scenarios with low antenna heights. The contribution of the scattering from these identified objects to the received power compared to other micromechanisms is evaluated. Results show that the scattering from these objects can be comparable to the wall reflections.**

***Index Terms*—Microcellular radio, propagation measurement, urban propagation channel.**

I. Introduction

URBAN mobile propagation channel has a complex physical nature. Dense building structures with irregular shapes and various materials, large number of mobile and static vehicles and pedestrians and finally the existence of various objects distributed in the area such as trees, signboards, traffic signs etc. make the urban radio propagation channel a complicated phenomena to investigate and model. Moreover, these environments are among the densest areas in the sense of mobile phone and other kinds of wireless devices' users. As a consequence, an extensive study of the urban wireless propagation channel is complicated but inevitable.

Recent researches on mobile radio channels have revealed that the received waves approach from finite distinct directions with different delays toward the receiver. This is because the scatterers are not usually distributed uniformly throughout the whole coverage area, but rather occur in clusters [1]–[4]. Furthermore, different measurement analyses in urban macrocell environments show that there are a few strong scatterers delivering a significant fraction of received power [5]–[7]. In macrocells it has always been assumed that building wall reflections and building corner and roof-edge diffractions are the dominant propagation micromechanisms, that is in small macrocellular environments the scatterers are basically building walls, building corners and building roof-edges.

On the other hand, some measurements assisted with high resolution data processing uncover that in the smaller cells, some objects other than buildings have been involved in the scattering of the received waves [8], [9]. Even in macrocell environment, scattering from lamppost has been reported [5] and the results of the research in [10] show that in small cell scenarios, the scattering from lampposts and traffic lights can be comparable to specular wall reflections and building edge diffractions in the urban areas. Consistent to these results, the performance of the radio propagation prediction tools have been reported to degrade due to scattering from objects other than buildings as trees or metal wire fences [11]. This is because in these prediction tools, the propagation micromechanisms are assumed to be specular reflections from smooth wall surfaces or diffraction from building edges but the existing scatterings from many irregular shaped objects are not included [12].

Toward a precise understanding of the microcell channel, further investigation and evaluation of different propagation micromechanisms in the urban areas is necessary. To fulfill this need, researches on non-specular scattering from building facades [13]–[16], and scattering from trees [17] have been done and the results were published recently. These are not however the only elements affecting the urban microcell channel. In a dense urban environment there are several other typical objects which can potentially cause scattering. The objective of this work is to identify these objects and to evaluate their contribution to the channel. The ultimate goal of the present research can be integration of the investigated micromechanisms in the ray tracing algorithms.

Before proceeding to the next sections it is necessary to specify the term "scattering from objects" used in this paper. As it was stated in the previous paragraph, the objective of this research is to analyze those propagation micromechanisms which exist in the urban propagation channel but are not included in the propagation prediction tools. These are mainly the contribution of the objects existing in the environment to the propagation channel. Depending on the object's size, shape, alignment and distance, this contribution can have any form of propagation mechanisms like reflection, scattering or diffraction. However for the sake of simplicity, we call it *scattering* from objects. In the following we will explain the measurement

Manuscript received September 15, 2005; revised May 31, 2006. This work was supported by NTT DoCoMo Inc.

M. Ghoraishi and J. Takada are with the Department of International Development Engineering, Tokyo Institute of Technology, Tokyo 152-8550, Japan (e-mail: mir@ap.ide.titech.ac.jp).

T. Imai is with the Research and Development Center, NTT DoCoMo, Inc., Kanagawa 238-0041, Japan

Digital Object Identifier 10.1109/TAP.2006.884238

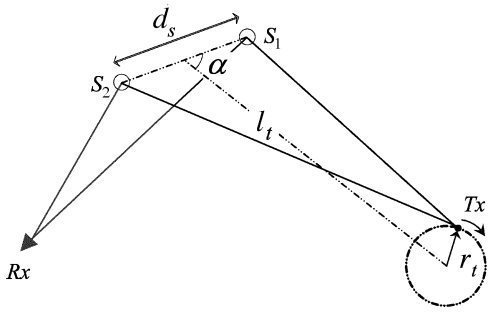

Fig. 1. The scenario of two objects separated d_s illuminated by a Tx antenna rotating with radius r_t. The midpoint of two objects is l_t far from the center of the Tx antenna rotation. The alignment of objects makes an angle of α with the l_t.

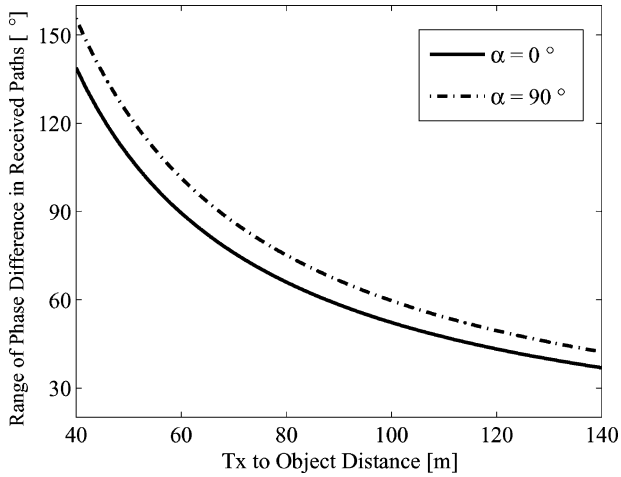

Fig. 2. The range of phase difference between two paths scattered by the objects of the scenario of Fig. 1 as a function of distance l_t for $\alpha = 0°$ and $\alpha = 90°$ where $2r_t = 0.5$ m and $d_s = 3.0$ m. The range of phase difference for other values of α lies between these two lines.

campaign in Section II. The method we have used to analyze the measurement data is then explained in Section III. In Section IV we will introduce several objects with strong influence on the channel and the impact of the scattering from objects on the channel is evaluated in Section V. Section VI is the conclusion.

II. Measurements

We have accomplished a series of measurements in a dense urban area in a small microcell scenario. The transmitter (Tx) and receiver (Rx) were in a line-of-sight (LoS) configuration. Both the Tx and Rx antennas were positioned at equal height of 3 m from the ground level.

A. Test Equipment

Antennas were mounted on the roof-tops of different cars at both Tx and Rx. The Tx employed a dipole sleeve antenna, and at the Rx a patch array as a directive antenna was used to detect the scatterers. Using a directive Tx antenna would have been advantageous to mitigate the interfering of the multipath scattered by different objects. However this causes a severe increase in the measurement time which makes the assumption of the static environment looser. Besides, as the devices are not absolutely time invariant, long measurement period is impractical. Consequently utilizing the directive antenna at the Tx for this measurement campaign was inappropriate.

The Tx dipole antenna was rotated with a diameter of 0.5 m and constant rotation speed of 5 rpm to create dynamic uncorrelated fading. This was done to average the multipath interference within the beam. Fig. 1 shows the scenario of two close objects S_1 and S_2 illuminated by the rotating Tx antenna. In this scenario, the midpoint of two scatterers is assumed to be in a distance of l_t from the Tx antenna rotation center. The alignment of two objects makes an angle of α to the l_t direction. Rotation of the Tx antenna causes a continuous change in the phase difference of the received paths scattered by these objects. Fig. 2 illustrates the range of this phase alteration when the objects are $d_s = 3.0$ m separated and the Tx antenna rotation diameter $2r_t = 0.5$ m as a function of l_t for $\alpha = 0°$ and $\alpha = 90°$. The range for other values of α lies between these two lines. Considering that two paths are resolvable if the phase difference is at least 90°, this figure shows that two objects of the scenario of Fig. 1 can produce resolvable paths if they are up to 70 m from the Tx antenna.

TABLE I
Measurement Specifications

f_c		3.35 GHz
Tx	Signal	BPSK, PN-9 Sequence
	Chip Rate	50 Mcps
	Power	40 dBm
	Antenna	Sleeve Dipole (2.2 dBi)
	Antenna Height	3 m
	Antenna Rotation	5 rpm Free Run
	Antenna Rotation Diameter	0.5 m
Rx	Antenna	Patch Array (24.5 dBi) 10° Beamwidths in Azimuth and Elevation Sidelobe Level -26 dB
	Antenna Height	3 m
	Antenna Rotation	3° Step (120 points for full azimuth)
Tx-Rx Separation		0.6 m

Measurements were accomplished by transmitting a PN-9 sequence of 50 Mcps corresponding to a path resolution of 6 m. At the Rx the received signal was captured in every 3° rotation of the directive antenna in the azimuth plane with vertical and horizontal beamwidths of 10°. The correlator outputs the instantaneous power-delay spectrum. By averaging 978 delay spectra for each direction in the azimuth plane, the power-delay profile was produced. Investigating these directional power-delay profiles, we are able to identify the clusters of the received waves in azimuth-delay domain. Table I shows the specifications of the experiments.

B. Measurement Sites

Dense urban areas near Kannai station in Yokohama city, Japan were chosen as the measurement sites. The data obtained from measurements in two different streets will be discussed.

Fig. 3. Measurement site location 1 north view.

Fig. 4. Measurement site location 2 east view.

A street of 26 m width [location 1 (L1)] and another nearby street of 18 m width [location 2 (L2)]. Figs. 3 and 4 show the views of the measurement environments and Figs. 5 and 6 show the layouts of the streets and measurement scenarios. For each measurement Tx and Rx were located 60 m apart in a LoS configuration and 5.5 m from walls of the same side. At location 1 two rounds of measurements were accomplished with Tx and Rx shifted 10 m each in the same direction for the second round keeping the Tx to Rx separation fixed to 60 m (points 1 and 2 (L1P1, L1P2)). At location 2 measurements were performed in 3 rounds. Tx and Rx were shifted 6 m each time in the same direction to keep the Tx to Rx separation at 60 m fixed [points 1, 2 and 3 (L2P1, L2P2, L2P3)]. In each of these points measurements were accomplished for full azimuth at every 3°.

At L1P2 and L2P3 just in between Tx and Rx, two roads with 13 m and 16 m width respectively were crossing the main streets so that there were no building to satisfy the specular reflection condition in these two points. A number of large trees existed along sidewalks in location 1 whereas the trees in location 2 were fewer and smaller. The measurements were accomplished in February with no leaves on the trees. Our observation shows that trees did not scatter any significant radio energy at the measurement time. The average building height in the area is estimated around 30 m. Measurements were accomplished during midnights with a very low traffic in the streets.

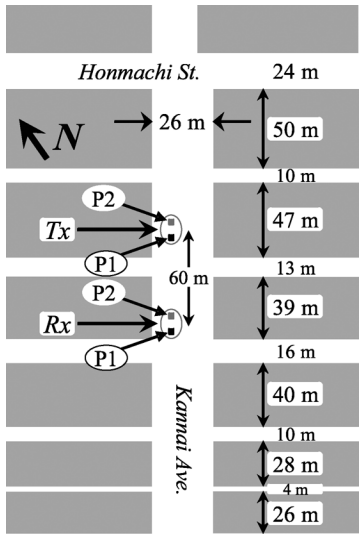

Fig. 5. Layout of the measurement site and scenarios at location 1.

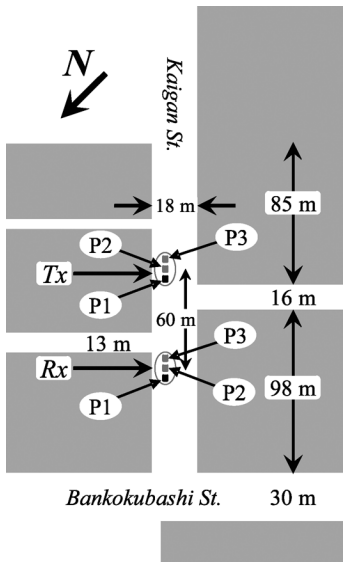

Fig. 6. Layout of the measurement site and scenarios at location 2.

III. Analysis Method

Precise maps of the areas are prepared. We include not only buildings but also every single object in the environment. The precise location of all objects have been measured by hand and included in the the maps. Major building facade irregularities are also included in the maps. Fig. 7 shows an example.

Apparently, reflection/scattering/diffraction points of all single-bounce receiving paths with the same delay but possibly different angles-of-arrival (AoA) have equal sum of distances from Tx and Rx. The locus of all these points in the azimuth plane is a horizontal ellipse. On the other hand the locus of last reflection/scattering/diffraction points of the paths with the same AoA but possibly different delays is a straight radial line originated at the Rx antenna. As a result we can grid the map by ellipses with Tx and Rx to be the ellipse foci and straight radial lines originated at Rx as is illustrated in Fig. 8. In this figure only a few ellipses have been shown for the sake of visibility. Then if we modify the delay scales in the

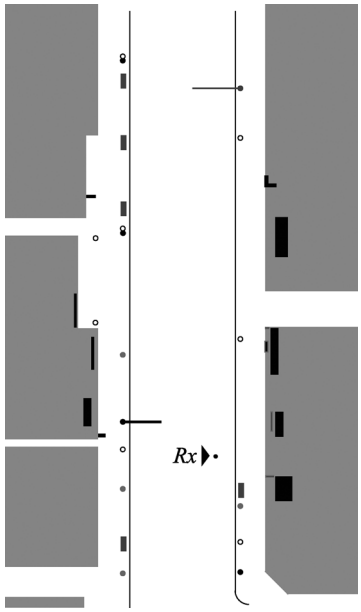

Fig. 7. An example of the map including all existing objects in the environment.

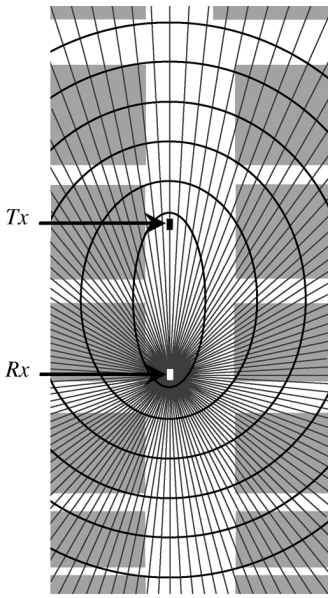

Fig. 8. An example of the gridded maps. Only a few ellipses have been shown for the sake of visibility.

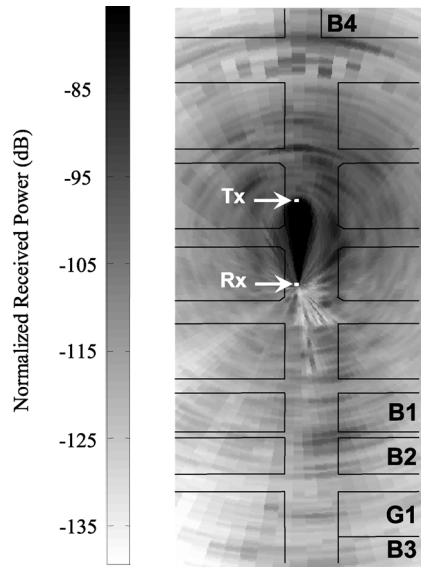

Fig. 9. The single-bounce scattering power distribution conforming to the map of the location 1 point 2 (L1P2).

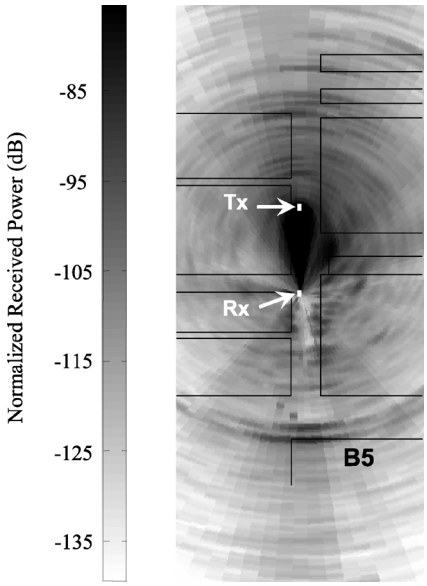

Fig. 10. The single-bounce scattering power distribution conforming to the map of the location 2 point 3 (L2P3).

measured power-delay profiles according to the elliptic grids, we can have the single-bounce scattering power distribution conforming to these grids. Fig. 9 shows an example of the result, that is the single-bounce scattering power distribution of the received signals at L1P2 whereas Fig. 10 shows the single-bounce scattering power distribution of the received signals at L2P3. As can be seen in these figures, the layout map of the area has been conformed with the single-bounce scattering power distribution. Using the gridded maps conformed to the single-bounce scattering power distribution we are able to identify the reflection/scattering/diffraction point of the single-bounce clustered received waves. It has to be noticed that this process is applicable only with the assumption of single-bounce. Thus those grids which are inside buildings or street canyons where there is no LoS to any of Tx or Rx can not be identified as any reflection/scattering/diffraction point with this method.

The outcome of the identification process of the scatterer objects will be discussed in the next section. The process itself is as following. For each cluster of the received waves we can find the corresponding scatterer object in the spatial resolution bin. There are some cases where more than one candidate as the sources of scattering lie in the same resolution bin. A candidate will be excluded from the list if any evidence proves its falling short of being the scattering source for the current measurement scenario, e.g. obstruction by another object. The elimination of all candidates but one leads us to the corresponding scattering source. There are yet few cases where more than one candidate survive up to the end of the process. If all of these candidates are

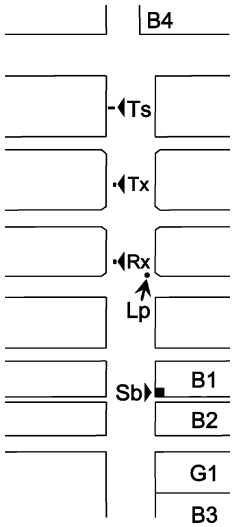

Fig. 11. Locations of the selected objects in the measurement location 1. The Tx and Rx locations are related to L1P2. Sb: signboard, Lp: lamppost, Ts: traffic sign, B1 and B2: two story buildings, B3: a ten story building, B4: a three story building, G1: open ground.

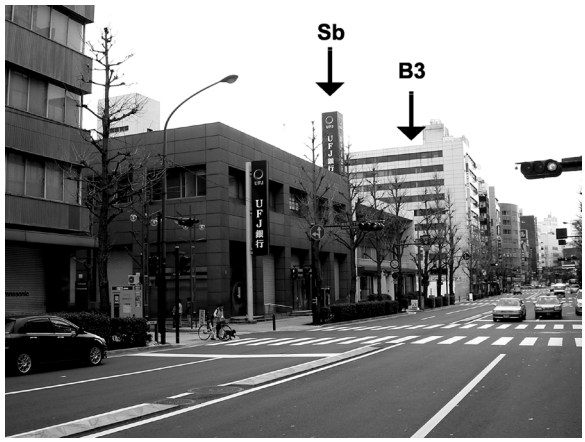

Fig. 12. The big signboard on the roof top of a two story building in location 1.

objects, even though they are not resolvable, the corresponding received cluster wave is considered as scattering from identified objects. This does not restrain the analysis conclusion as the objective is to investigate the contribution of the scatterings from all existing objects in the channel to the received power. Last point we would like to stress here is that the measurements were accomplished in more than one point in each location while all measurement parameters including the Tx to Rx distance is kept fixed. This helps to increase the certainty of the identified scattering points for the received clustered waves.

IV. Identified Objects

A number of different visible objects could be identified as sources of scattering by the method explained in the previous section [18]. Some other clusters, such as those inside the building zones, could not be identified as the scatterers considering the height of the buildings. They shall be due to multiscattered components. In this section we introduce a few of the identified objects. We do not however provide the details of the analysis for every identified object due to the limited space of the paper. The contributed loss L_s for each scatterer has been calculated in dB scales as following:

$$L_s = P_{ta} - P_r + G_t + G_r - L_0 - L_r \tag{1}$$

where P_{ta} is the transmitted power measured at the Tx antenna, P_r is the received power, G_t and G_r are the Tx antenna and Rx antenna gains respectively, L_r is the Rx cable loss and L_0 is the free space loss with respect to the propagation distance.

1) Signboard, Location 1: The first object to be introduced in this section is a big signboard mounted on the roof-top of a two story building. The dimensions of the signboard are 1.5 m in width and 6 m in height. In Fig. 11 the location of signboard is illustrated with Sb and Fig. 12 shows the picture of the signboard from the Rx direction. From Fig. 9 it is clearly visible that from the location of this signboard in the azimuth a significant amount of power is scattered toward Rx. The scattering source candidates for this cluster are the signboard and the corner of the building where the signboard is mounted on. However because of its grazing angle toward Tx and Rx and its low height, the building edge can not be the source of strong scattering power. Our experience shows that a building edge can scatter strong waves toward Rx only if it is visibly protruded into the street, e.g., B4 in Fig. 9. The contributed loss for this signboard is 13 dB.

To clarify the importance of such scattering source identification, we would like to carefully investigate the situation for this case. As it is clear from Fig. 11 the white building B3 at the background of the picture of Fig. 12 has the same alignment and visibility to Tx and Rx as the signboard. Also it must be noticed that B1 and B2 are two story buildings, G1 is an open ground and B3 is a 10 story tall building. Unexpectedly, it can be clearly understood from Fig. 9 that the signboard is scattering a significant amount of power but not much reflections from B3 is detected. This shows the drawback of the propagation tools, i.e. ray tracing algorithms, as in such tools 3-dimensional building map of the area is used but not any other object as signboards is considered in the simulation.

2) Lamppost (Street Light), Location 1: Many lampposts can be found in any urban area. Our measurement results show that lampposts scatter significant amount of high frequency radio waves. Fig. 13 shows the picture of one of the lampposts located close to the Rx. As the sidewalk is 4.5 m in width the visible building edge in the picture is resolvable from the lamppost. There is a big tree close to the lamppost, but as discussed in Section III no significant contribution from trees to the propagation channel was observed in our measurements. The contributed loss for this object was 12 dB. In Fig. 11 the location of this lamppost is demonstrated as Lp.

3) Traffic Sign, Location 1: The other common object in urban areas is traffic sign. Fig. 14 shows the picture of a traffic sign with a significant scattering effect. There is a tree in the spatial resolution bin which is rejected as the source of any significant scattering for the previously mentioned reason. The dimensions of this traffic sign are 1.5 m in width and 0.8 m in

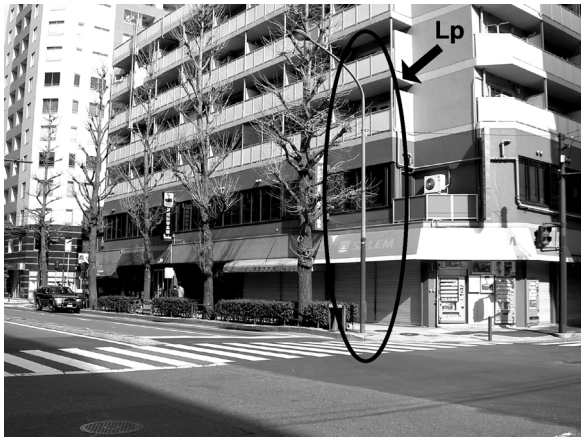

Fig. 13. A lamppost close to the Rx in location 1.

Fig. 14. A traffic sign from location 1.

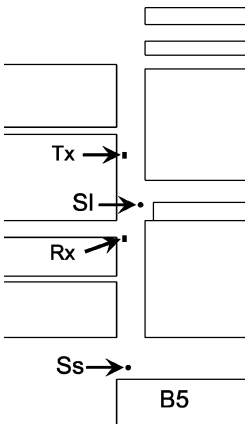

Fig. 15. Locations of the selected objects in the measurement location 2. The Tx and Rx locations are related to L2P3. Ss: a set of signboards, Sl: a traffic light, a street radar and a small traffic sign, B5: a four story building.

height and the contributed loss is 12 dB. Fig. 11 illustrates the location of this traffic sign with Ts letters.

4) Signboards, Location 2: From location 2 we introduce three signboards shown in Fig. 16. As these objects are not resolvable, all are considered as a set of scattering objects. This set is scattering a strong amount of energy because its alignment

Fig. 16. A set of signboards from location 2.

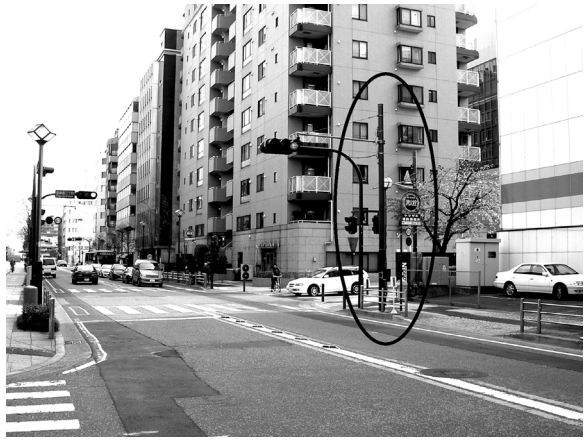

Fig. 17. A traffic light, a street radar and a small traffic sign from location 2.

TABLE II
DESCRIPTION OF IDENTIFIED OBJECTS

Identified objects description	No in location 1	No in location 2
Signboard	15	8
Lamppost (Street light)	7	14
Traffic sign	10	10
Traffic light	10	2
Cable box	0	3
Vending machine	0	2
Others	4	15

makes a specular reflection. The full height of the signboard at the right is 3.5 m and its maximum width is 2 m. The location of this set is in front of the building B5 in a distance of 9 m from the building. The strong cluster made by this set is well visible in Fig. 10 and its location is illustrated in Fig. 15 by Ss. The total contributed loss is 9 dB.

5) Traffic Light, Street Radar, Location 2: Next example from location 2 is a traffic light and a street radar plus a small traffic sign. These are in the same resolution bin but are well resolvable from buildings and objects around them. Their location is illustrated in Fig. 15 by Sl and Fig. 17 shows the objects. The height of the street radar pole is 5 m and of the street light is 4 m. The total contributed loss is 11 dB.

TABLE III
PROPAGATION MICROMECHANISM CONTRIBUTIONS TO THE RECEIVED POWER

Propagation Micromechanism	L1 P1	L2 P1	L2 P2	L1 P2	L2 P3
Specular Wall Reflection	existed			did not exist	
LoS Component	70%	53%	64%	74%	84%
Scattering from Identified Objects	6%	15%	9%	6%	7%
Wall Reflection	14%	19%	15%	4%	4%
Clustered Multiscattered Received Waves	3%	9%	10%	7%	3%
Unidentified	7%	3%	2%	9%	2%
Contribution of Scattering from Identified Objects to non-LoS component	20%	32%	25%	23%	44%

V. EVALUATION

The analysis of the measurement results shows that a significant amount of received power has been scattered by the objects which we have identified in this work [19]. These objects are signboards, lampposts, traffic signs, traffic lights, electricity cable boxes, vending machines and generally any metallic object with dimensions of several tens of wavelengths in the vicinity of any of Tx or Rx up to 100 m. Table II shows the list of these objects and their numbers in each of the measurement locations.

In location 1 identified scatterers are distributed over a larger area. This is because the street is wider. Big signboards and relatively close lampposts are among the strong scatterers in this area. In location 2 some building irregularities have caused strong scattering effects. Besides, we observe scattering from cable boxes and vending machines in this location as well.

Table III shows the contribution of propagation micromechanisms for the measurements. Clustered multiscattered received waves are those clusters which lie within the building zone in the single-bounce scattering power distribution when it is conformed to the map of the measurement area, thus the scattering source for these clusters can not be identified because of the single-bounce assumption. The contribution of the scattering from identified objects to the non-LoS received signals is at least 20% in any of the measurement points. For any of L1P2 and L2P3 as it was mentioned earlier there was not any specular wall reflection and therefore the wall reflected received power is lower than other cases. As it is clear from the data given in the table, the wall reflection component can vary dramatically based on the existence of the specular reflection and the street width.

In Figs. 18 and 19 we have illustrated the contribution of the propagation micromechanisms in the channel to the non-LoS received power. In Fig. 18 the values are averaged over three measurement points L1P1, L2P1 and L2P2 where specular wall reflection existed in the channel and for Fig. 19 the values have been averaged over two measurement points L1P2 and L2P3 where there is not any specular wall reflection in the channel. The results of these figures and of Table III indicate that in situations where there is not any specular wall reflection in the channel the scattering from objects can be comparable to the single-bounce wall reflections and in any case is significant. In our measurements this value could be as high as 44% of the non-LoS component for L2P3 case.

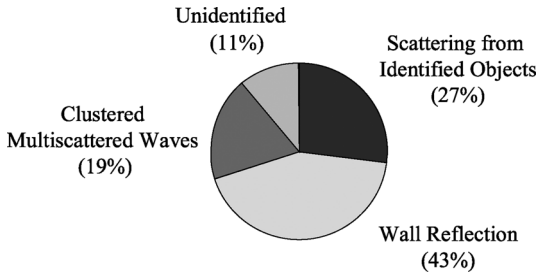

Fig. 18. Non-LoS received power contributions averaged for the three measurement point scenarios where specular wall reflections existed.

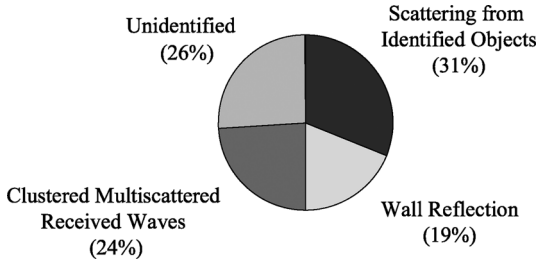

Fig. 19. Non-LoS received power contributions averaged for the two measurement point scenarios without any specular wall reflections.

VI. CONCLUSION

This research shows that the metallic objects with dimensions as small as tens of radio wavelengths can be the source of a significant amount of scattering in the urban microcell propagation channel. That is any metallic object like signboards, lampposts, traffic signs, traffic lights, electricity cable boxes and vending machines in the vicinity of any of Tx or Rx up to 100 m is a potential source of significant scattering in the wireless radio propagation channel. We evaluated this effect for single-bounce received waves in two dense urban areas where measurements were performed in 5 points. Results show that in the locations where there is not any specular wall reflection in the channel the scattering from these objects can be comparable to wall reflection and in any case it has a significant contribution to the non-LoS received waves. Any prediction of the urban propagation channel needs to carefully consider and evaluate these scattering effects. Especially it has to be considered in the future ray tracing algorithms applied to urban areas.

ACKNOWLEDGMENT

The authors would like to thank NTT DoCoMo Inc. for its support of this project.

REFERENCES

[1] H. Asplund, A. Molisch, M. Steinbauer, and N. Mehta, "Clustering of scatterers in mobile radio channels-evaluation and modeling in the COST259 directional channel model," in *Proc. IEEE Int. Conf. Commun. (ICC 2002)*, Apr. 2002, vol. 2, pp. 901–905.

[2] J. Fuhl, J. Rossi, and E. Bonek, "High-resolution 3D direction-of-arrival determination for urban mobile radio," *IEEE Trans. Antennas Propag.*, vol. 45, pp. 672–683, Apr. 1997.

[3] U. Martin, "Spatio-temporal radio channel characteristics in urban macrocells," *IEE Proc. Radar, Sonar, Navig.*, vol. 145, no. 1, pp. 42–49, Feb. 1998.

[4] Y. Oda and T. Taga, "Clustering of local scattered multipath components in urban mobile environments," in *Proc. IEEE Veh. Technol. Conf. (VTC'02 Spring)*, May 2002, vol. 1, pp. 11–15.

[5] K. Kalliola, H. Laitinen, P. Vainikainen, M. Toeltsch, J. Laurila, and E. Bonek, "3-D double-directional radio channel characterization for urban macrocellular applications," *IEEE Trans. Antennas Propag.*, vol. 51, no. 11, pp. 3122–3233, Nov. 2003.

[6] J. Laurila, K. Kalliola, M. Toeltsch, K. Hugl, P. Vainikainen, and E. Bonek, "Wideband 3D characterization of mobile radio channels in urban environment," *IEEE Trans. Antennas Propag.*, vol. 50, no. 2, pp. 233–243, Feb. 2002.

[7] L. Vuokko, P. Vainikainen, and J. Takada, "Clusters extracted from measured propagation channels in macrocellular environments," *IEEE Trans. Antennas Propag.*, vol. 53, no. 12, pp. 4089–4098, Dec. 2005.

[8] E. Bonek, H. Hofstetter, C. Mecklenbrauker, and M. Steinbauer, "Double-directional superresolution radio channel measurements," presented at the Proc. 39th Allerton Conf. on Communication, Control, and Computing, Allerton, Oct. 3–5, 2001.

[9] B. Fleury, X. Yin, K. Rohbrandt, P. Jourdan, and A. Stucki, "Performance of a high-resolution scheme for joint estimation of delay and bidirection dispersion in the radio channel," in *Proc. IEEE Veh. Technol. Conf. (VTC'02 Spring)*, May 2002, vol. 1, pp. 522–526.

[10] K. Rizk, J. Wagen, J. Li, and F. Gardiol, "Lamppost and panel scattering compared to building reflection and diffraction," COST259, TD(97) May 1996.

[11] S. Kim, B. Guarino, T. Willis, V. Erceg, S. Fortune, R. Valenzuela, L. Thomas, J. Ling, and J. Moore, "Radio propagation measurements and prediction using three-dimensional ray tracing in urban environments at 908 MHz and 1.9 GHz," *IEEE Trans. Veh. Technol.*, vol. 48, no. 3, pp. 931–946, May 1999.

[12] H. Li, C. Chen, T. Liu, and H. Lin, "Applicability of ray-tracing technique for the prediction of outdoor channel characteristics," *IEEE Trans. Veh. Technol.*, vol. 49, no. 6, pp. 2336–2349, Nov. 2000.

[13] H. Budiarto, K. Horihata, K. Haneda, and J. Takada, "Experimental study of non-specular wave scattering from building surface roughness for the mobile propagation modeling," *IEICE Trans. Commun.*, vol. E87-B, no. 4, pp. 958–966, Apr. 2004.

[14] C. Constantinou and M. Mughal, "On the modeling of reflected energy from building faces in microcellular mobile radio planning tools," *IEEE Trans. Antennas Propag.*, vol. 53, no. 8, pp. 2623–2630, Aug. 2005.

[15] V. Degli-Esposti, D. Guiducci, A. de'Marsi, P. Azzi, and F. Fuschini, "An advanced field prediction model including diffuse scattering," *IEEE Trans. Antennas Propag.*, vol. 52, no. 7, pp. 1717–1728, Jul. 2004.

[16] P. Pongsilamanee and H. Bertoni, "Specular and nonspecular scattering from building facades," *IEEE Trans. Antennas Propag.*, vol. 52, no. 7, pp. 1879–1889, Jul. 2004.

[17] Y. de Jong and M. Herben, "A tree-scattering model for improved propagation prediction in urban microcells," *IEEE Trans. Veh. Technol.*, vol. 53, no. 2, pp. 503–513, Mar. 2004.

[18] M. Ghoraishi, J. Takada, and T. Imai, "Investigating dominant scatterers in urban mobile propagation channel," in *Proc. IEEE Int. Symp. Commun. Information Technology (ISCIT 2004)*, Oct. 2004, vol. 1, pp. 154–158.

[19] ——, "Microcell urban propagation channel analysis using measurement data," in *Proc. IEEE Veh. Technol. Conf. (VTC'05 Fall)*, Sep. 2005, vol. 3, pp. 1728–1731.

Mir Ghoraishi (S'99–M'05) received the B.E. degree from Isfahan University of Technology, Esfahan, Iran, and the M.E. degree from Amirkabir University of Technology, Tehran, Iran, in 1993 and 1999, respectively, both in electrical engineering.

In 1999, he entered Tokyo Institute of Technology for a Ph.D. course where he was a Research Assistant from 2004 to 2006. Since 2006, he has been a Researcher with Tokyo Institute of Technology. His research interests are wireless radio propagation channel measurement and modeling and rough surface scattering analysis and modeling.

Mr. Ghoraishi is a member of the Institute of Electronics, Information and Communication Engineers of Japan (IEICE).

Junichi Takada (S'89–M'93) received the B.E., M.E., and D.E. degrees from the Tokyo Institute of Technology, Tokyo, Japan, in 1987, 1989, and 1992, respectively.

From 1992 to 1994, he was a Research Associate Professor with Chiba University, Chiba, Japan. From 1994 to 2006, he was an Associate Professor with Tokyo Institute of Technology, where, since 2006, he has been a Professor. His current interests are wireless propagation and channel modeling, array signal processing, UWB radio, cognitive radio, applied radio instrumentation and measurements, and ICT for international development.

Dr. Takada is a member of IEICE, ACES, and the ECTI Association Thailand.

Tetsuro Imai (M'93) was born in Tochigi, Japan, in 1967. He received the B.S. and Ph.D. degrees from Tohoku University, Sendai, Japan, in 1991 and 2002, respectively.

He joined the Wireless System Laboratories of Nippon Telegraph and Telephone Corporation (NTT), Kanagawa, Japan, in 1991. Since then, he has been engaged in the research and development of radio propagation and system design for mobile communications. He is now Manager of the Radio Access Network Development Department, NTT DoCoMo, Inc., Kanagawa, Japan.

Dr. Imai is a Member of the Institute of Electronics, Information and Communication Engineers of Japan (IEICE).